Real-space Eliashberg approach to charge order of electrons coupled to dynamic antiferromagnetic fluctuations

Real space Eliashberg approach to charge order of electrons coupled to dynamic antiferromagnetic fluctuations

Johannes Bauer[1] and Subir Sachdev[1,2]
[1] *Department of Physics, Harvard University, Cambridge, Massachusetts 02138, USA and*
[2] *Perimeter Institute for Theoretical Physics, Waterloo, Ontario N2L 2Y5, Canada*
(Dated: June 23, 2015)

We study charge ordered solutions for fermions on a square lattice interacting with dynamic antiferromagnetic fluctuations. Our approach is based on real space Eliashberg equations which are solved self-consistently. We first show that the antiferromagnetic fluctuations can induce arc features in the spectral functions, as spectral weight is suppressed at the hot spots; however, no real pseudogap is generated. At low temperature spontaneous charge order with a d-form factor can be stabilized for certain parameters. As long as the interacting Fermi surfaces possesses hot spots, the ordering wave vector corresponds to the diagonal connection of the hot spots, similar to the non-self-consistent case. Tendencies towards observed axial order only appear in situations without hot spots.

PACS numbers: 71.10.Fd,74.72.-h,71.27.+a

I. INTRODUCTION

Signatures of charge order in the copper-oxide based superconductors have attracted a lot of recent attraction. By now charge ordered states have become an essential ingredient of the phase diagram for the different families.[1,2] Whilst in La-based compounds charge and spin stripe order have a considerable history,[3–5] it was only firmly established in recent years in other cuprate families. Early reports include scanning tunneling microscopy (STM) studies,[6–9] followed by bulk property measurements by resonant X-ray scattering (REXS).[10–12] The order has a finite correlation length in zero magnetic field and becomes long range ordered at high magnetic fields.[13,14] This helps to understand previously puzzling quantum oscillation data.[15–17]

By now the charge order has been carefully characterized experimentally. It is unconventional in the sense that it possess an incommensurate wave length $\lambda = 3 - 4a$, where a is the Cu-Cu distance in the copper oxide planes and an internal form factor. In both STM and REXS the direction of the wave vector has been established as pointing along the axes in the Cu-Cu square lattice, $\boldsymbol{Q} = Q_0(1,0)$.[10,11,18,19] Its magnitude follows the Fermi surface, or more precisely, Fermi arc evolution; concretely this means that it decreases with increasing hole doping.[18] This suggests that the order is connected to Fermi surface properties and can possibly be understood as a Fermi surface instability.[18,19] In contrast, in La-based compounds the ordering wave vector shows the opposite trend, and $\boldsymbol{Q}$ increases with increasing hole doping.[20,21] Recent experiments have revealed further details of the charge order in Bi- and Y-based compounds. Both STM and REXS data are well understood based on a d-form factor as an internal structure for the order.[22–24]

Many theories have addressed the microscopic origin of the charge order including its onset temperature, its wave vector, form factor and dependence on doping and magnetic field.[2,25–30,30–35] One line of reasoning starts with fermions interacting with antiferromagnetic spin fluctuations peaked at wave vector $\boldsymbol{K}$ (see Fig. 1).[28,36–39] The hot spot model with linearized dispersion has a strong nesting instability with a diagonal wave vector $\boldsymbol{Q} = Q_0(1,1)$ connecting the hot spots (see Fig. 1).[36] In models starting with an intact Fermi surface this instability is at least as strong as the one with an axial wave vector $\boldsymbol{Q} = Q_0(1,0)$, and it is therefore difficult to explain the experiments based on such a theory. A number of recent works have explored situations where the non-interacting Fermi surface has been modified due to magnetic order and pocket formation[40–42] or pseudogap features.[43] It has been argued that it is important to take such features into account, such that the dominant instability can be altered. Also fluctuation effects,[44–47] strong correlation effects,[38,39] and starting points of fractional Fermi liquids[48] have been considered as a possibility to favor axial order over the diagonal one.

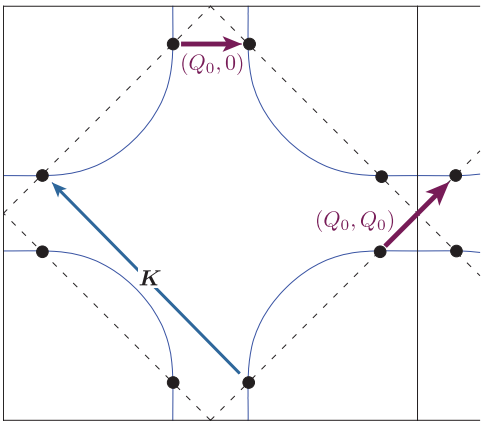

FIG. 1: (Color online) Schematic picture of Fermi surface with antiferromagnetic wave vector connecting hot spots $\boldsymbol{K}$ and examples of diagonal, $\boldsymbol{Q} = Q_0(1,1)$, and axial, $\boldsymbol{Q} = Q_0(1,0)$, charge ordering wave vectors.

The main idea of this work is to analyze whether single particle self-energy modification, due to a coupling to

dynamic spin fluctuations, and without appeal to more exotic states, is sufficient to establish charge order with properties as observed in experiments. Our analysis will be carried out with a semi-phenomenological model of fermions coupled to dynamic spin fluctuations, also called spin-fermion model in the literature. Such a model is appealing as it naturally captures the d-wave superconductivity in a range of dopings.[49,50] We show that in the relevant doping regime for charge order, dynamic magnetic fluctuations with a finite correlation length $\xi \sim 2a$ are a more realistic description for the cuprates than including static magnetic order.[40,41] To analyze the model, we use a real space formulation which allows us to probe charge order directly in the ordered phase. Our formulation also allows for simple extensions to include impurities or disorder, spin order, coupling to phonons, superconducting order, and a magnetic field. The paper is structured as follows: In Sec. II we describe the details of the model and approach. In Sec. III we analyze ordered solutions in the static limit in order to connect to previous work. In Sec. IV we analyze the full dynamic model before concluding in Sec. V.

II. MODEL DEFINITION AND REAL SPACE ELIASHBERG APPROACH

We use a model with the action of the form,[49,50]

$$\begin{aligned} S &= -\sum_{\sigma}\sum_{ij,n}\overline{\psi}_{i,\sigma}(i\omega_n)G^{-1}_{ij,0}(i\omega_n)\psi_{j,\sigma}(i\omega_n) \qquad (1)\\ &- \frac{g^2}{2}\sum_{i,j}\int \mathrm{d}\tau \int \mathrm{d}\tau'\ \chi(\boldsymbol{r}_i-\boldsymbol{r}_j,\tau-\tau')\boldsymbol{S}(\boldsymbol{r}_i,\tau)\cdot\boldsymbol{S}(\boldsymbol{r}_j,\tau'), \end{aligned}$$

where

$$G_{ij,0}(i\omega_m)^{-1} = (i\omega_m+\mu)\delta_{ij} - t_{ij}, \qquad (2)$$

and

$$S^{\alpha}(\boldsymbol{r}_i,\tau) = \overline{\psi}_{i,\sigma_1}(\tau)\sigma^{\alpha}_{\sigma_1,\sigma_2}\psi_{i,\sigma_2}(\tau). \qquad (3)$$

Here, $\psi_{i,\sigma}$ is a fermionic field for site i and spin label σ. The non-interacting dispersion in momentum space is

$$\begin{aligned}\varepsilon_{\boldsymbol{k}} &= -2t_1[\cos(k_1)+\cos(k_2)] - 4t_2\cos(k_1)\cos(k_2)\\ &\quad -2t_3[\cos(2k_1)+\cos(2k_2)],\end{aligned}$$

where the copper-copper lattice spacing is set to $a=1$.

For the spin-fluctuation spectrum we assume,[49–51]

$$\chi(\boldsymbol{q},i\omega_m) = \frac{a_\chi}{N_K}\sum_{i=1}^{N_K}\frac{1}{\omega_{\boldsymbol{K}_i}(\boldsymbol{q}) + a_{v_s}^2\omega_m^2 + \frac{|\omega_m|}{\omega_{\mathrm{sf}}}}. \qquad (4)$$

To preserve lattice periodicity we define $\omega_{\boldsymbol{K}_i}(\boldsymbol{q}) = 2(2-\cos(q_x-\boldsymbol{K}_{x,i})-\cos(q_y-\boldsymbol{K}_{y,i}))+\Gamma^2$, and we usually take for simplicity $\boldsymbol{K}=(\pi,\pi)$. Γ is directly related to the correlation length $\Gamma=\xi^{-1}$. For $a_{v_s}=0$ this form is common in the literature such as in the well-known work of Millis *et al.*[51] and fits experimental data from neutron scattering well. In real space we have

$$\chi(\boldsymbol{r}_i-\boldsymbol{r}_j,i\omega_m) = \frac{1}{N_s}\sum_{\boldsymbol{q}}\chi(\boldsymbol{q},i\omega_m)\mathrm{e}^{i\boldsymbol{q}(\boldsymbol{r}_i-\boldsymbol{r}_j)}, \qquad (5)$$

where N_s is the number of lattice sites.

a. Real space equations - The basic equation for the Eliashberg approach is

$$\Sigma_{ij}(i\omega_n) = 3Tg^2\sum_m \chi(\boldsymbol{r}_i-\boldsymbol{r}_j,i\omega_n-i\omega_m)G_{ij}(i\omega_m), \qquad (6)$$

where G is the full Green's function. We assume that no spin order occurs and omit spin labels on G and Σ. In order to compute Σ self-consistently we also need to solve the Dyson equation,

$$G_{ij}(i\omega_m)^{-1} = (i\omega_m+\mu)\delta_{ij} - t_{ij} - h_{ij} - \Sigma_{ij}(i\omega_m). \qquad (7)$$

When working in real space $G_{ij}(i\omega_m)$ can be obtained by matrix inversion for each $i\omega_m$, a computation which can be easily parallelized. The calculation of Σ in Eq. (6) can also be parallelized well. In the Green's function G in Eq. (7), we have included a general symmetry breaking field, which can be introduced into the Hamiltonian by

$$H_{\mathrm{co}} = \sum_{i,j,\sigma} h_{ij}c^{\dagger}_{i,\sigma}c_{j,\sigma}. \qquad (8)$$

In order to find inhomogeneous solutions we have to initialize the calculations with such a field. We assume that χ in Eq. (4) is fixed by the input parameters and not further renormalized in a self-consistent manner. We work on a two-dimensional lattice with $N_s = N_1\times N_1$ sites and periodic boundary conditions.

b. Homogeneous case - In the homogeneous situation G and Σ only depend on $\boldsymbol{r}_i-\boldsymbol{r}_j$. With a Fourier transform we can then write,

$$\Sigma_{\boldsymbol{k}}(i\omega_n) = 3g^2T\sum_{m,\boldsymbol{q}}\chi(\boldsymbol{k}-\boldsymbol{q},i\omega_n-i\omega_m)G(\boldsymbol{q},i\omega_m) \qquad (9)$$

and the Dyson equation can be solved explicitly,

$$G_{\boldsymbol{k}}(i\omega_m) = \frac{1}{i\omega_m - \varepsilon_{\boldsymbol{k}} + \mu - \Sigma_{\boldsymbol{k}}(i\omega_m)}. \qquad (10)$$

In the spectral representation we have

$$\begin{aligned}\Sigma_{\boldsymbol{k}}(i\omega_n) &= 3g^2\sum_{\boldsymbol{q}}\int \mathrm{d}\omega_1\int \mathrm{d}\omega_2\ \frac{\rho_\chi(\boldsymbol{k}-\boldsymbol{q},\omega_1)\rho_G(\boldsymbol{q},\omega_2)}{i\omega_n-\omega_1-\omega_2}\\ &\quad\times[n_{\mathrm{F}}(\omega_2)+n_{\mathrm{B}}(-\omega_1)],\end{aligned}$$

where $\rho_\chi(\boldsymbol{q},\omega)$ is the spectral function for the spin-fluctuation spectrum, and $n_{\mathrm{F}}(\omega)$, $n_{\mathrm{B}}(\omega)$ denote the

fermionic and bosonic distribution functions, respectively. Analytic continuation, $i\omega \to \omega + i\eta$, yields the imaginary part of the self-energy

$$\mathrm{Im}\Sigma_{\boldsymbol{k}}(\omega) = -3\pi g^2 \sum_{\boldsymbol{q}} \int \mathrm{d}\omega_2 \; \rho_\chi(\boldsymbol{k}-\boldsymbol{q}, \omega-\omega_2)\rho_G(\boldsymbol{q},\omega_2) \times [n_{\mathrm{F}}(\omega_2) + n_{\mathrm{B}}(\omega_2-\omega)]. \quad (11)$$

and the real part can be computed from the Kramers-Kronig transformation. From this the electronic spectral function $\rho_G(\boldsymbol{k},\omega)$ can be computed. For a numerical calculation it is favorable to use the real space form for the self-energy equation and switch to momentum space by Fast Fourier transforms.

c. Charge order observables - For the order parameter we focus on the inhomogeneous part of

$$\Delta_{ij} = \sum_\sigma \langle c^\dagger_{i,\sigma} c_{j,\sigma}\rangle = \sum_{\boldsymbol{Q}} \Big[\frac{1}{V}\sum_{\boldsymbol{k}} \Delta_{\boldsymbol{Q}}(\boldsymbol{k}) \mathrm{e}^{i\boldsymbol{k}\boldsymbol{r}}\Big] \mathrm{e}^{i\boldsymbol{Q}\boldsymbol{R}}. \quad (12)$$

where $\boldsymbol{r} = \boldsymbol{r}_i - \boldsymbol{r}_j$ and $\boldsymbol{R} = (\boldsymbol{r}_i + \boldsymbol{r}_j)/2$. Given a spin-diagonal Green's function $G_{ij}(i\omega_n)$ we can compute $\Delta_{ij} = 2T\sum_n G_{ij}(i\omega_n)\mathrm{e}^{i\omega_n\tau^-}$, $\tau^- \to 0$. To extract the inhomogeneous part Δ^{ih} we map it to coordinates $\boldsymbol{R}$, $\boldsymbol{r}$, $\Delta_{ij} \to \Delta(\boldsymbol{R},\boldsymbol{r})$ and then compute $\Delta(\boldsymbol{r}) = \Delta(\boldsymbol{R},\boldsymbol{r}) - \frac{1}{N_R}\sum_{\boldsymbol{R}}\Delta(\boldsymbol{R},\boldsymbol{r})$. Then we find $\Delta^{\mathrm{ih}}(\boldsymbol{R},\boldsymbol{r}) = \Delta(\boldsymbol{R},\boldsymbol{r}) - \Delta(\boldsymbol{r})$. Without any charge order symmetry breaking Δ^{ih} is zero.

We assume that the inhomogeneous part $\Delta^{\mathrm{ih}}_{\boldsymbol{Q}}(\boldsymbol{k})$ can be expanded as

$$\Delta^{\mathrm{ih}}_{\boldsymbol{Q}}(\boldsymbol{k}) = \sum_n a_n(\boldsymbol{Q}) f_n(\boldsymbol{k}), \quad (13)$$

with a suitable set of orthonormal basis functions $\{f_n(\boldsymbol{k})\}$. The explicit form of the relevant functions used here can be found in the appendix. These can be transformed to the real space representation,

$$f_n(\boldsymbol{r}) = \frac{1}{N_s}\sum_{\boldsymbol{k}} f_n(\boldsymbol{k})\mathrm{e}^{-i\boldsymbol{k}\boldsymbol{r}}. \quad (14)$$

For a given function $\Delta^{\mathrm{ih}}(\boldsymbol{R},\boldsymbol{r})$, the coefficients $a_n(\boldsymbol{Q})$ can be calculated from

$$a_n(\boldsymbol{Q}) = \sum_{\boldsymbol{R},\boldsymbol{r}} \Delta^{\mathrm{ih}}(\boldsymbol{R},\boldsymbol{r})\mathrm{e}^{-i\boldsymbol{Q}\boldsymbol{R}} f_n(\boldsymbol{r}). \quad (15)$$

d. Parameters of the model - The model in Eq. (1) contains a number of parameters, which we summarize here for clarity. The bare electronic structure is determined by the hoppings t_1, t_2 and t_3, and the filling $n = 1/N_s\sum_{i,\sigma} n_{i,\sigma}$ by the chemical potential μ. Unless otherwise mentioned $t_1 = 1$ sets the energy scale. To get a rough idea about absolute scales we can think of a typical identification $t_1 \simeq 300$meV$\simeq 3481$K; however, we make no attempt for a quantitative theory in comparison with experiment here. The spin fluctuation spectrum has the following parameters: the overall weight factor a_χ, the inverse correlation length $\Gamma = \xi^{-1}$, the spin fluctuation scale ω_{sf} and the ω^2 coefficient a_{v_s}. We use parameters similar to the recent work of Mishra and Norman.[34] In addition we have the temperature T, where the lowest value reached is $T = 0.02t_1$ ($\simeq 70$K). Moreover we have a coupling constant g. A technical parameter is the size of the real space lattice. We did most of our calculations for $N_1 = 32$. The limit for this is set by memory constraints.

III. RESULTS FOR THE STATIC MODEL

We first consider the situation where the spin-fluctuation spectrum is a static, which corresponds to the limit $\omega_{\mathrm{sf}} \to \infty$ and $a_{v_s} \to 0$ in Eq. (4). This helps us to connect to previous results[28] and test our formalism and procedure. The equation for the self-energy then simplifies to,

$$\Sigma_{ij} = 3g^2\chi(\boldsymbol{r}_i - \boldsymbol{r}_j)\frac{\Delta_{ij}}{2}. \quad (16)$$

This purely static renormalization does not lead to any quasiparticle damping. However, it leads to a sizeable renormalization of the chemical potential and hopping parameters. Using the relative coordinate $\boldsymbol{r} = \boldsymbol{r}_i - \boldsymbol{r}_j$, we can relate the renormalized parameters $\{\mu, t_i\}$ to the bare ones $\{\mu_0, t_i^0\}$ by $\mu = \mu_0 + \Sigma(\boldsymbol{r}=0)$, $t_1 = t_1^0 + \Sigma(|\boldsymbol{r}|=1)$ $t_2 = t_2^0 + \Sigma(|\boldsymbol{r}| = \sqrt{2})$, and $t_3 = t_3^0 + \Sigma(|\boldsymbol{r}|=2)$, where t_i^0 are the bare parameters.

In our procedure we search for spontaneously ordered solutions of the self-consistency equations (6) and (7) by initializing the calculations by a random field h_{ij} [see Eq. (8)]. This is initially included in the Green's function in Eq. (7) and then set to zero from the second iteration on. We use a real space lattice with $N_1 = 32$ sites in one direction and iteratively calculate the full Green's function G_{ij} and self-energy Σ_{ij}. Some mixing of iterations and initial onsite homogenization is used to improve convergence. One example for a charge order solution is obtained with the parameter set $t_1^0 = 0.764$, $t_2^0 = -0.33$, $t_3^0 = 0.154$, and $\mu_0 = 0.393$. For $T = 0.05$, $\Gamma = \xi^{-1} = 0.5$, and $g^2 = 3$, we obtain $t_1 \approx 1.0$, $t_2 \approx -0.32$, $t_3 \approx 0.11$, $\mu \approx -1.1$, and the renormalized Fermi surface looks very similar to Fig. 1. From the converged result for G_{ij}, the expectation values Δ_{ij} and $\Delta^{\mathrm{ih}}_{ij}$ are obtained as described in Sec. II. In Fig. 2, we plot the result for the nearest neighbor bonds in $x-$ and $y-$direction as obtained from $\Delta^{\mathrm{ih}}_{ij}$. This shows how an ordering pattern spontaneously appears and is stabilized after 30 iterations.

The properties of the ordering pattern can either be identified directly from the real space representation in Fig. 2 or well understood by the decomposition into the basis function, Eq. (15). The largest coefficients are shown in Fig. 3. For simplicity, we only show the coefficients for a series of momenta $\boldsymbol{Q} = (Q_x, Q_y)$ in the triangle, $Q_x \in [0,\pi]$, $Q_y \in [0, Q_x]$, labeled by n_Q.

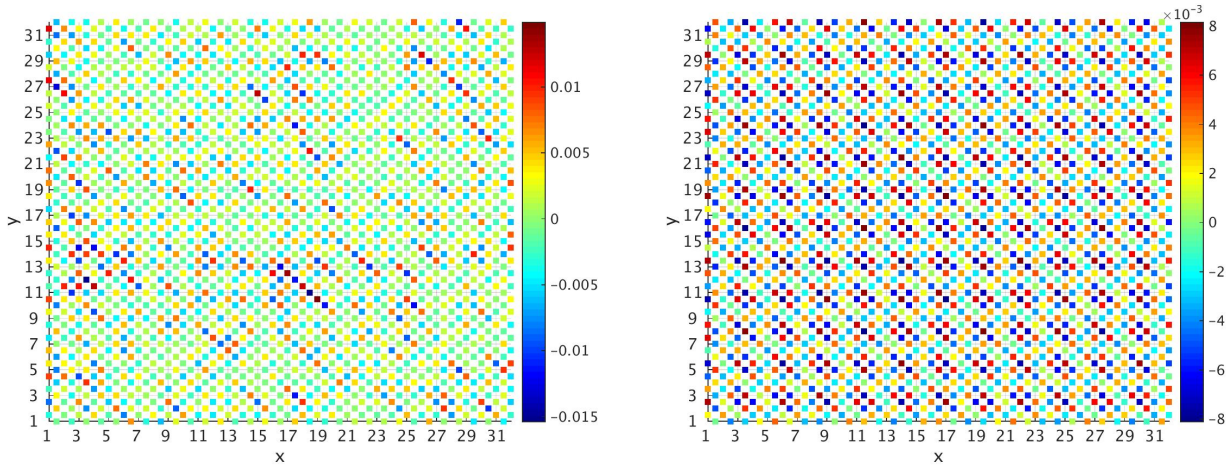

FIG. 2: (Color online) Results for the static model. We plot the nearest neighbor bond values of $\Delta_{ij}^{\rm ih}$ on a real space lattice initialized by a random field after 5 iterations (left) and spontaneously ordered results after 30 iterations (right).

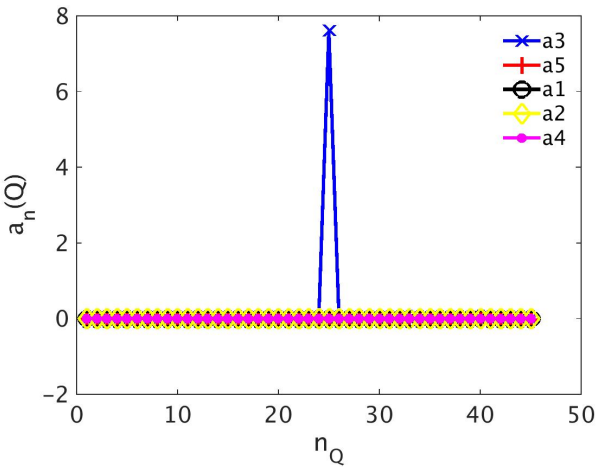

FIG. 3: (Color online) Plot of the largest $a_n(\boldsymbol{Q})$ for different basis functions ($n = 1, \ldots, 13$). The values of $\boldsymbol{Q}$ are labeled by $n_{\boldsymbol{Q}}$, where $n_{\boldsymbol{Q}} = 25$ corresponds to $\boldsymbol{Q} = Q_0(1,1)$, with $Q_0 = 3/8$ in units π/a. This value agrees well with the diagonal distance between hot spots.

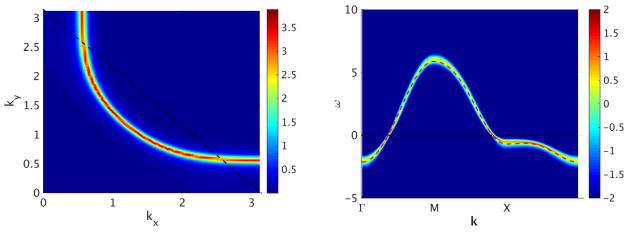

FIG. 4: (Color online) Plot of interacting Fermi surface in the dynamic model with weak coupling, $g = 1.0$. We plot the spectral density ($\rho_{\boldsymbol{k}}(\omega = 0)$) (left) and renormalized band structure ($\log \rho_{\boldsymbol{k}}(\omega)$ for clarity) for $\boldsymbol{k}$ along the trajectory $\Gamma \to M \to X \to \Gamma$ (right). The dashed line gives the non-interacting dispersion. The parameter values are given in the text.

There is a clear maximum for a_3 for $n_{\boldsymbol{Q}} = 25$ which corresponds to $\boldsymbol{Q} = Q_0(1,1)$, with $Q_0 = 3/8 = 0.375$ in units π/a. This value agrees well with the diagonal distance between the hot spots on the Fermi surface, and the ordering form factor is of the d-wave form, $n = 3$, $f_3(\boldsymbol{k}) = \cos k_x - \cos k_y$ (see Table I in the appendix). As mentioned we only show the result for a restricted set of $\boldsymbol{Q}$ vectors. The order in Fig. 1 is really a superposition of $\pm(Q_x, Q_y)$, $\pm(Q_x, -Q_y)$ wave vectors. We conclude that our real space Eliashberg calculations are consistent with earlier work based on an instability analysis.[28] The $\boldsymbol{k}$-space resolution for the finite size lattice is sufficient to resolve these features and the relation to the Fermi surface. The dominant instability is realized here as an ordered solution.

IV. RESULTS FOR DYNAMIC MODEL

A. Homogeneous situation

As discussed in the last section, in the static limit self-energy corrections only lead to a renormalization of the hoppings, but do not lead to any damping of quasi-particles. For a dynamic interaction such as in Eq. (4) the effect is different.[52–55] In fact, this one of the major aspects of our work to include those effects on the single particle level. Scattering is particularly strong at the hot spots such that quasi-particle excitations can become suppressed. Here, we would like to investigate the effect of this on the charge order instabilities. The basic questions are: How much is the diagonal order suppressed by the self-energy effects? Can the axial order become favorable over the diagonal one? In order to get some insights about the effects on the Fermi surface, we first consider the homogeneous situation and solve the Eliashberg equations self-consistently on the real frequency axis, Eq. (11). For clarity we first show results for weak interaction $g = 1$. The other model parameters

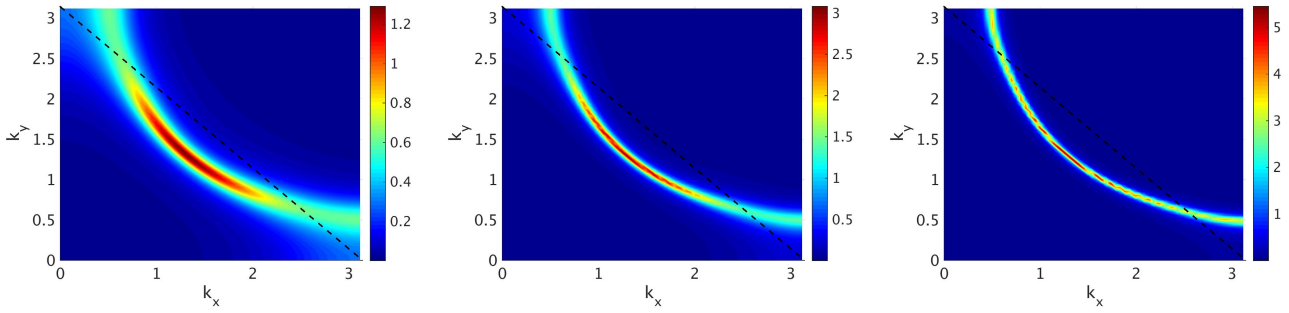

FIG. 5: (Color online) Plot of interacting Fermi surface ($\rho_{\boldsymbol{k}}(\omega = 0)$) at strong coupling $g = 5.0$ for $T = 0.1, 0.05, 0.02$ (left to right.)

are $t_1^0 = 1$, $t_2^0 = -0.32$, $t_3^0 = 0.11$, $\mu_0 = -1.1$, $\omega_{\rm sf} = 0.5$, $a_{v_s} = 1$, $\Gamma = 0.5$, and $T = 0.05$. The result for the interacting Fermi surface, $\rho_{\boldsymbol{k}}(\omega = 0)$, for one part of the Brillouin zone is shown in Fig. 4 (left).

A broadening value $\eta = 0.08$ was used to enhance clarity for the given $\boldsymbol{k}$-space resolution. Not surprisingly, the result resembles very much the non-interacting Fermi surface. On the right in Fig. 4 we also display $\rho_{\boldsymbol{k}}(\omega)$ for $\boldsymbol{k} = (k_x, k_y)$ on the trajectory $(0,0) \to (\pi,\pi) \to (0,\pi) \to (0,0)$ ($\Gamma \to M \to X \to \Gamma$), which gives insights on the damping and renormalized band structure. We have added the non-interacting dispersion as a dashed line. Here again the result is almost identical with the non-interacting case.

We also show the results for a stronger interacting case $g = 5$ in Fig. 5, where $\mu = -1$ and we show the temperatures $T = 0.1, 0.05, 0.02$. Here, $\eta = 0.05$ was chosen in the analytical continuation for the broadening.

As we can see in Fig. 5 the thermal part of the spin fluctuation spectrum can give considerable effects on the electronic spectrum and give features resemblant of Fermi arcs, which have been observed in experiments.[56] The effect is more pronounced for larger temperature as can also be deduced from Eq. (11). Hence, spectral weight is suppressed close to the hot spots where the scattering with the spin-fluctuations is particularly strong. Stronger arc-like features can be realized for larger values of the correlation length ξ, i.e., smaller values of Γ. It is worth noting that non-selfconsistent calculations also give stronger arc features. However, self-consistent Eliashberg equations generically do not produce real pseudogap features.[50,54,55]

In Fig. 6 we show for $T = 0.05$ the renormalized band structure. We find effects of Fermi velocity renormalization and redistribution of spectral weight. As we will discuss below this has consequences for the instability analysis and realization of ordered phases.

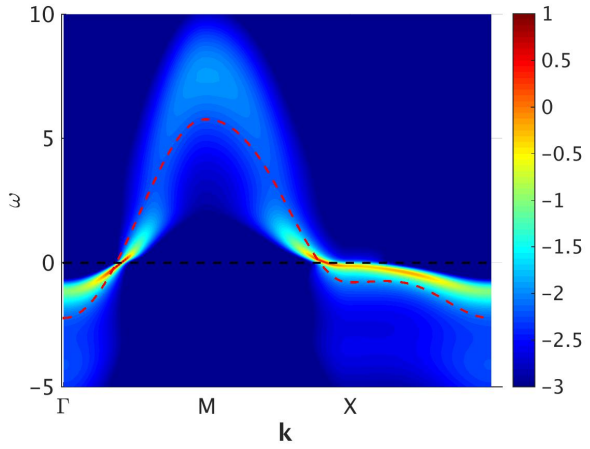

FIG. 6: (Color online) Plot of renormalized band structure ($\log \rho_{\boldsymbol{k}}(\omega)$ for clarity) at strong coupling $g = 5.0$. Other model parameter as described in the text.

B. Spontaneous order

Within a similar procedure as described in Sec. III, we have done extensive calculations to check for charge order solution for the model with the dynamic interaction. The calculations were done for a real space lattice with $N_1 = 32$ and a grid of Matsubara frequency large enough to capture relevant features. A random field h_{ij} is used for initialization. In the appendix, we describe some results which were obtained from calculations with field induced order. For most calculations we used the hopping parameters $t_1^0 = 1$, $t_2^0 = -0.32$, and $t_3^0 = 0.11$. By varying μ_0, we analyzed parameters with filling factors $n \sim 0.8 - 0.95$ and temperatures down to $T = 0.02$ in units of t_1^0. The parameters of the spin fluctuation spectrum where varied in a regime $\omega_{\rm sf} \sim 0.2 - 1$, and $\Gamma = 1/2$ and $\Gamma = 1/4$ was analyzed; we usually kept $a_{v_s} = a_\chi = 1$. We also scanned a range of coupling strengths g.

Generally, we found the appearance of the charge order to be strongly suppressed in a scheme with dynamic spin fluctuations as compared to the static case. One reason is the finite extent of the interaction in frequency space in contrast to the static case. Another reason is the single-particle renormalization effect of the self-energy. Charge order enters via an inhomogeneous modulation of $\Sigma_{ij}(i\omega_n)$ in the self-consistent calculation, which appears on top of generic variation of $\Sigma_{ij}(i\omega_n)$ as function of $\boldsymbol{r}_i - \boldsymbol{r}_j$. This ordering tendency should be enhanced with the coupling g. However, the self-energy also has

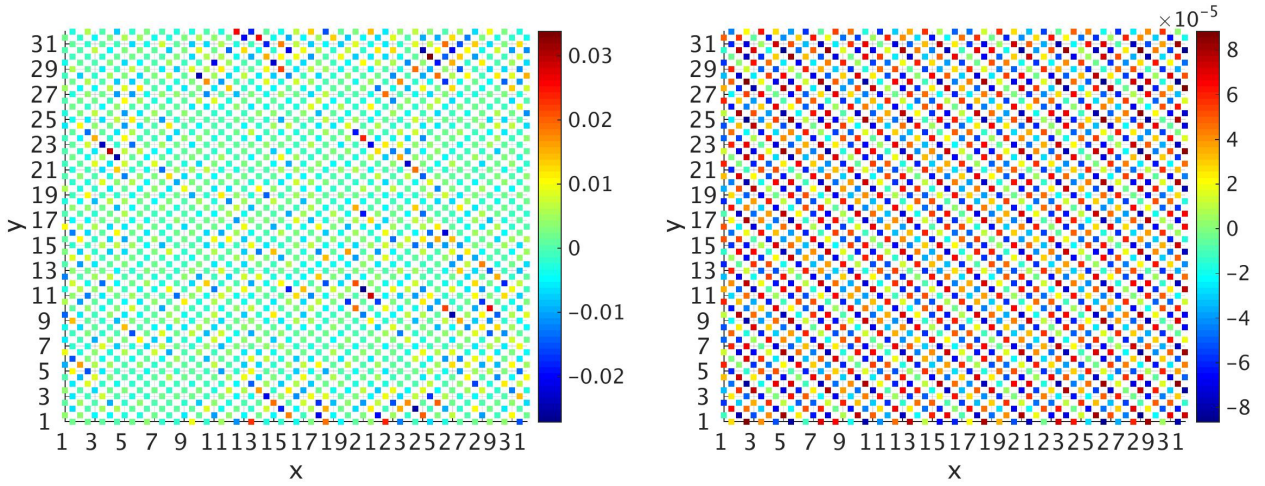

FIG. 7: (Color online) Nearest neighbor bond values of $\Delta_{ij}^{\rm ih}$ on real space lattice initialized by a random field after 5 iterations (left) and spontaneously ordered results after 45 iterations (right). Model parameter as described in the text.

an effect to damp and renormalize single particle excitation, which leads to the opposite effect of a suppression of the order. This is a generic feature, which also appears for other Fermi surface instabilities, such as superconductivity. As a consequence for many of the probed parameters no charge ordered solution could be stabilized, even though some ordering features appear in intermediate values of the iterations. For instance, for $T = 0.05$ we did not find spontaneously ordered solutions for any of the parameters tested.

In Fig. 7, we present the result of a calculation at $T = 0.02$, where spontaneous charge order appears in the self-consistent Eliashberg equations. The parameters are $\omega_{\rm sf} = 0.5$, $\Gamma = 0.5$, with a coupling $g = 5$. Since $\chi(\boldsymbol{r}_i - \boldsymbol{r}_j, i\omega_m)$ is fairly small this coupling strength is not as large as it might appear; for instance, the nearest neighbor self-energy reaches maximal values $|{\rm Re}\Sigma(\boldsymbol{r}_i, \boldsymbol{r}_i + \hat{x}, i\omega_n)| \sim 0.2$ for these parameters. We show a result for $\mu_0 = -1$, which correspond to a filling of $n \simeq 0.92$ for the interacting system. The calculations are again initialized by a random field and the spontaneous ordering pattern visible after 45 iterations is seen on the right in Fig. 7. The corresponding Fourier analysis is displayed in Fig. 8.

As in the static case we find a dominant d-form factor, $n = 3$ and a diagonal wave vector with magnitude $\boldsymbol{Q} = Q_0(1, 1)$, with $Q_0 = 3/8$. There is also a minor component for $n = 7$, where $f_7(\boldsymbol{k}) = \cos(2k_x) - \cos(2k_y)$. The wave vector matches the connection of the hot spots of the interacting Fermi surface well (as seen in Fig. 5). The diagonal order is dominant even though the spectral density is substantially suppressed near the hot spots. For different filling factors, we also find diagonal order, whenever a hot spot is present in the interacting Fermi surface, and the length of the wave vector changes accordingly.

In situations where there are no hot spots visible in the interacting Fermi surface, for instance, when the filling

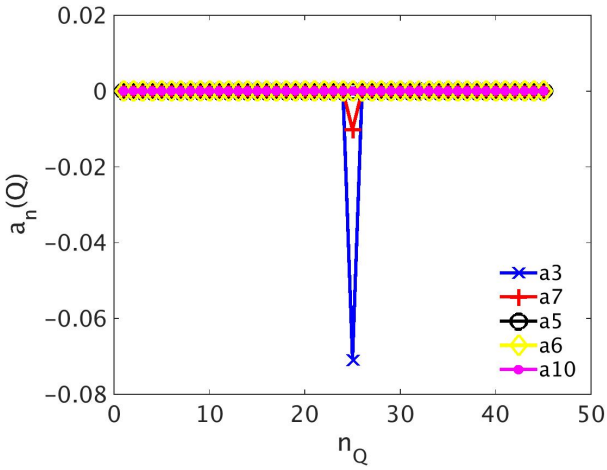

FIG. 8: (Color online) Plot of the largest $a_n(\boldsymbol{Q})$ for different basis functions ($n = 1, \ldots, 13$). The values of $\boldsymbol{Q}$ are label by $n_{\boldsymbol{Q}}$, where $n_{\boldsymbol{Q}} = 25$ corresponds to $\boldsymbol{Q} = Q_0(1, 1)$, with $Q_0 = 3/8$ in units π/a. This value agrees well with the diagonal distance between hot spots.

is lowered such the Fermi surface becomes closed around $(0, 0)$, we found solutions with ordering tendencies with wave vector along the axis. The dominant form factor is $n = 3$, the d-form factor. For filling $T = 0.02$, $n \sim 0.8$ the wave vector $\boldsymbol{Q} = Q_0(1, 0)$, with $Q_0 = 1/2$ can be found, which is very similar to the experimental wave length $\lambda \sim 4$. The order is, however, quite small and not well established. It is possible that lower temperatures and additional ingredients are needed to stabilize the order well.

V. DISCUSSION AND CONCLUSIONS

Based on a model of fermions on a square lattice interacting with dynamic antiferromagnetic interactions,

we have analyzed general charge order solutions. We used self-consistent Eliashberg equations to compute self-energies and spectral functions. We showed that the spectral functions can be substantially modified in the interacting theory. In particular, structures resembling Fermi arcs can appear due to the strong scattering around the hot spots. However, no real pseudogap features are generated by self-consistent Eliashberg equations.

The appearance of charge order is studied based on a real space version of the Eliashberg equations, which are initialized by a random field. We only found spontaneously ordered solutions at low temperature, *e.g.*, $T = 0.02t_1$, and for relatively large interaction strengths. Generically, the charge order posses a d-form factor and a diagonal wave vector related to the hot spots of the interacting Fermi surface. This result is in line with a number of previous studies,[2,28,29,34,37–39] many of which however did not include dynamic interactions and self-energy effects, and studied instabilities from the normal state rather than ordered solutions. One of our main results is that the suppression of spectral weight at the hot spots by the dynamic model is not large enough to alter the behavior of the charge order. For large dopings, when the interacting Fermi surface has no hot spots, we found tendencies towards order with wave vector along the axis. This finding is in line with studies suppressing the hot spots, for instance, by pocket formation or including a phenomenological pseudogap.[40–43,48]

In relation to the observation of charge order in the cuprate superconductors, we find a number of features consistent with the experiments. These include the dominant d-form factor and the behavior of $\boldsymbol{Q}$ with doping. The direction of the wave vector is, however, not correctly reproduced. This is likely related to the fact that the self-consistent Eliashberg theory does not include strong enough pseudogap features, and therefore still supports an instability related to the hot spot. As such, the present approach does not provide a comprehensive explanation for the experimental findings. Nevertheless, with suitable modifications our real space Eliashberg approach might useful for future applications, as it can easily be extended to include superconductivity, magnetic field effects, impurity effects, coupling to phonons and spin order.

Acknowledgments - We wish to thank A. Allais, D. Chowdhury, A.J. Millis, M. Norman, M. Punk, P. Strack for fruitful discussions. JB would like to thank the Deutsche Forschungsgemeinschaft for support through grant number BA 4371/1-1. This research was supported by the NSF under Grant DMR-1360789, the Templeton foundation, and MURI grant W911NF-14-1-0003 from ARO. Research at Perimeter Institute is supported by the Government of Canada through Industry Canada and by the Province of Ontario through the Ministry of Research and Innovation.

n	$f_n(\boldsymbol{k})$
1	1
2	$\cos k_x + \cos k_y$
3	$\cos k_x - \cos k_y$
4	$\sin k_x + \sin k_y$
5	$\sin k_x - \sin k_y$
6	$\cos(2k_x) + \cos(2k_y)$
7	$\cos(2k_x) - \cos(2k_y)$
8	$\sin(2k_x) + \sin(2k_y)$
9	$\sin(2k_x) - \sin(2k_y)$
10	$2\cos k_x \cos k_y$
11	$2\sin k_x \sin k_y$
12	$2\sin k_x \cos k_y$
13	$2\cos k_x \sin k_y$

TABLE I: Relevant basis functions

Appendix

1. Basis functions

Here we collect the basis functions which were used for the charge order analysis. We focused on the 13 basis functions $f_n(\boldsymbol{k})$ as shown in Table I. The corresponding function of the real space representation $f_n(\boldsymbol{r})$ can be easily calculated analytically from Eq. (14). They include form factors up to next-nearest neighbors. Higher order functions could be in principle be considered but they do not play a role in our analysis. These functions $f_n(\boldsymbol{r})$ are used to compute the coefficients $a_n(\boldsymbol{Q})$ in Eq. (15).

2. Field induced order

Here, we briefly summarize some results from a complementary analysis to Sec. IV. We studied charge order when a small finite field is present in the self-consistent calculations. We focused on the situation with d-form factor and assumed $\phi_3(\boldsymbol{Q}) = \phi_3(-\boldsymbol{Q})$. We chose $\phi_3(\boldsymbol{Q}) = 0.001$ keeping the field finite in (7) during the self-consistent calculation and scanned over various vectors $\boldsymbol{Q}$. A response function characteristic of the susceptility to charge order can be defined as $\chi(n, \boldsymbol{Q}) = \frac{\delta a_n(\boldsymbol{Q})}{\delta \phi_n(\boldsymbol{Q})}$.

First of all we can consider the situation for $g = 0$, such that $\Sigma_{ij} = 0$. Clearly there cannot be spontaneous order in this situation, however, the susceptibility for different wave vectors can be analyzed. We find that the field induced order as measured by $\chi^0(3, \boldsymbol{Q})$ is strongest for $\boldsymbol{Q}_d = (Q_0, Q_0)$, where Q_0 approximately connects the hot spots, and there is also a local maximum along the Q_x axis, for $\boldsymbol{Q}_a = (Q_0, 0)$. Within the real space calculations with $N_1 = 32$ one finds $\chi^0(3, \boldsymbol{Q}_a)/\chi^0(3, \boldsymbol{Q}_d) \simeq 0.78$. Hence the diagonal order is favored. These results are clearly expected from the instability analysis based on unrenormalized fermions[28] where these quantities can be

computed from the corresponding fermionic bubbles and form factors.

For finite g the self-energy effects play an important role. As discussed the ordering tendency is induced form an inhomogeneous contribution of the real part of $\Sigma_{ij}(i\omega_n)$. In contrast to the static case $\Sigma_{ij}(i\omega_n) \to 0$ for large $i\omega_n$ so this is only a contribution at small ω_n. However, the self-energy also produces other effects, such as renormalization of the band and suppression and shift of spectral weight as already discussed in the section on the homogeneous calculations. These effects mostly lead to a reduction of the ordering tendency. This is in fact common for weak coupling instabilities which are strongest without self-energy corrections. Hence, the combination of these effects means that the field induced ordering susceptility is not necessarily enhanced for finite g. In our analysis for different parameters and interactions we found that typically $\chi(3, \boldsymbol{Q}_d)$ with the diagonal wave-vector is largest and can be enhanced over the non-interacting value. For the parameters studied diagonal response was found to be larger than the $\chi(3, \boldsymbol{Q}_a)$, i.e., instabilities along the axial direction, consistent with what has been discussed in the main text.

[1] E. Fradkin and S. A. Kivelson, Nature Physics **8**, 864 (2012).
[2] B. Keimer, S. Kivelson, M. Norman, S. Uchida, and J. Zaanen, Nature **518**, 179 (2015).
[3] J. Tranquada, B. Sternlieb, J. Axe, Y. Nakamura, and S. Uchida, Nature **375**, 561 (1995).
[4] V. J. Emery, S. A. Kivelson, and J. M. Tranquada, Proc. Natl. Acad. Sci. (USA) **96**, 8814 (1999).
[5] S. A. Kivelson, I. P. Bindloss, E. Fradkin, V. Oganesyan, J. M. Tranquada, A. Kapitulnik, and C. Howald, Rev. Mod. Phys. **75**, 1201 (2003).
[6] J. Hoffman, E. Hudson, K. Lang, V. Madhavan, H. Eisaki, S. Uchida, and J. Davis, Science **295**, 466 (2002).
[7] M. Vershinin, S. Misra, S. Ono, Y. Abe, Y. Ando, and A. Yazdani, Science **303**, 1995 (2004).
[8] Y. Kohsaka, C. Taylor, K. Fujita, A. Schmidt, C. Lupien, T. Hanaguri, M. Azuma, M. Takano, H. Eisaki, H. Takagi, et al., Science **315**, 1380 (2007).
[9] M. Lawler, K. Fujita, J. Lee, A. Schmidt, Y. Kohsaka, C. K. Kim, H. Eisaki, S. Uchida, J. Davis, J. Sethna, et al., Nature **466**, 347 (2010).
[10] G. Ghiringhelli, M. Le Tacon, M. Minola, S. Blanco-Canosa, C. Mazzoli, N. Brookes, G. De Luca, A. Frano, D. Hawthorn, F. He, et al., Science **337**, 821 (2012).
[11] J. Chang, E. Blackburn, A. Holmes, N. Christensen, J. Larsen, J. Mesot, R. Liang, D. Bonn, W. Hardy, A. Watenphul, et al., Nature Physics **8**, 871 (2012).
[12] A. J. Achkar, R. Sutarto, X. Mao, F. He, A. Frano, S. Blanco-Canosa, M. Le Tacon, G. Ghiringhelli, L. Braicovich, M. Minola, et al., Phys. Rev. Lett. **109**, 167001 (2012).
[13] T. Wu, H. Mayaffre, S. Krämer, M. Horvatić, C. Berthier, W. Hardy, R. Liang, D. Bonn, and M.-H. Julien, Nature **477**, 191 (2011).
[14] D. LeBoeuf, S. Krämer, W. Hardy, R. Liang, D. Bonn, and C. Proust, Nature Physics **9**, 79 (2013).
[15] N. Doiron-Leyraud, C. Proust, D. LeBoeuf, J. Levallois, J.-B. Bonnemaison, R. Liang, D. Bonn, W. Hardy, and L. Taillefer, Nature **447**, 565 (2007).
[16] S. E. Sebastian, N. Harrison, and G. G. Lonzarich, Rep. Prog. Phys. **75**, 102501 (2012).
[17] A. Allais, D. Chowdhury, and S. Sachdev, Nature communications **5** (2014).
[18] R. Comin, A. Frano, M. Yee, Y. Yoshida, H. Eisaki, E. Schierle, E. Weschke, R. Sutarto, F. He, A. Soumyanarayanan, et al., Science **343**, 390 (2014).
[19] E. H. da Silva Neto, P. Aynajian, A. Frano, R. Comin, E. Schierle, E. Weschke, A. Gyenis, J. Wen, J. Schneeloch, Z. Xu, et al., Science **343**, 393 (2014).
[20] M. Hücker, M. v. Zimmermann, G. D. Gu, Z. J. Xu, J. S. Wen, G. Xu, H. J. Kang, A. Zheludev, and J. M. Tranquada, Phys. Rev. B **83**, 104506 (2011).
[21] J. M. Tranquada, in *American Institute of Physics Conference Series* (2013), vol. 1550, pp. 114–187.
[22] K. Fujita, M. H. Hamidian, S. D. Edkins, C. K. Kim, Y. Kohsaka, M. Azuma, M. Takano, H. Takagi, H. Eisaki, S.-i. Uchida, et al., Proc. Nat. Acad. Sci. **111**, E3026 (2014).
[23] R. Comin, R. Sutarto, F. He, E. H. da Silva Neto, L. Chauviere, A. Frano, R. Liang, W. N. Hardy, D. A. Bonn, Y. Yoshida, et al., Nat. Mater. **advance online publication** (2015), URL `http://dx.doi.org/10.1038/nmat4295`.
[24] M. H. Hamidian, S. D. Edkins, C. K. Kim, J. C. Davis, A. P. Mackenzie, H. Eisaki, S. Uchida, M. J. Lawler, E.-A. Kim, S. Sachdev, et al., to appear (2015).
[25] T. Holder and W. Metzner, Phys. Rev. B **85**, 165130 (2012).
[26] C. Husemann and W. Metzner, Phys. Rev. B **86**, 085113 (2012).
[27] M. Bejas, A. Greco, and H. Yamase, Phys. Rev. B **86**, 224509 (2012).
[28] S. Sachdev and R. La Placa, Phys. Rev. Lett. **111**, 027202 (2013).
[29] Y. Wang and A. Chubukov, Phys. Rev. B **90**, 035149 (2014).
[30] T. A. Maier and D. J. Scalapino, Phys. Rev. B **90**, 174510 (2014).
[31] A. M. Tsvelik and A. V. Chubukov, Phys. Rev. B **89**, 184515 (2014).
[32] P. A. Lee, Phys. Rev. X **4**, 031017 (2014).
[33] V. S. de Carvalho and H. Freire, Annals of Physics **348**, 32 (2014), ISSN 0003-4916.
[34] V. Mishra and M. R. Norman, ArXiv e-prints (2015), 1502.02782.
[35] Y. Wang and A. Chubukov, Phys. Rev. B **91**, 195113 (2015).
[36] M. A. Metlitski and S. Sachdev, Phys. Rev. B **82**, 075128 (2010).
[37] J. D. Sau and S. Sachdev, Phys. Rev. B **89**, 075129 (2014).
[38] A. Allais, J. Bauer, and S. Sachdev, Indian Journal of Physics pp. 1–9 (2014), ISSN 0973-1458.

[39] A. Allais, J. Bauer, and S. Sachdev, Phys. Rev. B **90**, 155114 (2014).
[40] S. Bulut, W. A. Atkinson, and A. P. Kampf, Phys. Rev. B **88**, 155132 (2013).
[41] W. Atkinson, A. Kampf, and S. Bulut, New Journal of Physics **17**, 013025 (2015).
[42] A. Thomson and S. Sachdev, Phys. Rev. B **91**, 115142 (2015).
[43] L. Zhang and J.-W. Mei, ArXiv e-prints (2014), 1408.6592.
[44] D. Chowdhury and S. Sachdev, Phys. Rev. B **90**, 134516 (2014).
[45] C. Pépin, V. S. de Carvalho, T. Kloss, and X. Montiel, Phys. Rev. B **90**, 195207 (2014).
[46] Y. Wang, D. F. Agterberg, and A. Chubukov, Phys. Rev. B **91**, 115103 (2015).
[47] M. Punk, Phys. Rev. B **91**, 115131 (2015).
[48] D. Chowdhury and S. Sachdev, Phys. Rev. B **90**, 245136 (2014).
[49] A. Abanov, A. V. Chubukov, and J. Schmalian, Advances in Physics **52**, 119 (2003).
[50] A. Chubukov, D. Pines, and J. Schmalian, in *Superconductivity (Vol 2)*, edited by K. Bennemann and J. Ketterson (Springer, Berlin, 2008).
[51] A. Millis, H. Monien, and D. Pines, Phys. Rev. B **42**, 167 (1990).
[52] A. Kampf and J. R. Schrieffer, Phys. Rev. B **41**, 6399 (1990).
[53] A. P. Kampf and J. R. Schrieffer, Phys. Rev. B **42**, 7967 (1990).
[54] J. Schmalian, D. Pines, and B. Stojković, Phys. Rev. Lett. **80**, 3839 (1998).
[55] J. Schmalian, D. Pines, and B. Stojković, Phys. Rev. B **60**, 667 (1999).
[56] K. M. Shen, F. Ronning, D. Lu, F. Baumberger, N. Ingle, W. Lee, W. Meevasana, Y. Kohsaka, M. Azuma, M. Takano, et al., Science **307**, 901 (2005).